International Journal of GEOMATE, Feb., 2024 Vol.26, Issue 114, pp.25-33
ISSN: 2186-2982 (P), 2186-2990 (O), Japan, DOI: https://doi.org/10.21660/2024.114.4082
Geotechnique, Construction Materials and Environment

SEISMIC VULNERABILITY ASSESSMENT USING THE HVSR METHOD AT YOGYAKARTA INTERNATIONAL AIRPORT UNDERPASS, INDONESIA

Anky Rakhmat Prasetya[1], *Fikri Faris[2] and Adam Pamudji Rahardjo[3]

[1,2,3] Department of Civil and Environmental Engineering, Faculty of Engineering, Universitas Gadjah Mada, Indonesia

*Corresponding Author, Received: 07 Aug. 2023, Revised: 23 Dec. 2023, Accepted: 28 Dec. 2023

ABSTRACT: The Underpass at Yogyakarta International Airport (YIA) is in the Temon District, Kulon Progo Regency, Yogyakarta Province, Indonesia. The YIA has become one of the focal points for national infrastructure development and economic growth. Based on historical seismic activity, YIA and its vicinity are characterized by high levels of seismic activity. However, the data and information available regarding this matter are notably limited. This research aims to assess the soil vulnerability in the vicinity of the YIA Underpass. The soil vulnerability assessment is conducted by measuring microtremors and groundwater levels. The microtremor data is processed using the Horizontal-to-Vertical Spectral Ratio (HVSR) method with geopsy software and guidelines provided by Site Effects Assessment Using Ambient Excitations (SESAME). The research findings reveal that the study area exhibits a high seismic hazard potential, as evidenced by the seismic vulnerability index (K_g), which is more than 20. The interpretation of the HVSR curve indicates that the study area is characterized by a low dominant frequency (f_0) ranging from 0.214 to 0.289 Hz, along with varying shear wave velocities. Based on the stress-corrected shear wave velocity (V_{s1}), point U01 is more likely to liquefy than U05 and U07 as V_{s1} in some soil layers is less than 215 m/s. This analysis indicates that the study area is susceptible to earthquake hazards due to thick soil deposit layers and shallow groundwater levels.

Keywords: Seismic vulnerability, Microtremor, Shear wave velocity, Soil classification, Liquefaction

1. INTRODUCTION

Kulon Progo and its surrounding area are characterized by high seismic activity. Records from the past two decades (2000-2023) show that 427 earthquakes with magnitudes greater than five have occurred near Java Island, as depicted in Fig.1. On May 26, 2006, a 6.3 Mw earthquake at a depth of 10 km struck Yogyakarta and its surrounding areas [1]. This event destroyed over 6700 houses and resulted in the death of 22 people in Kulon Progo Regency [2]. However, earthquake data for this region are either nonexistent or, if available, are subject to proprietary restrictions.

Presently, a portion of the agricultural area in Kulon Progo Regency has been transformed into the national strategic project of Yogyakarta International Airport (YIA). Kulon Progo has transitioned into the concept of an aerotropolis [3]. YIA was completed in mid-2019, while the YIA Underpass was completed at the end of 2019. The existence of YIA has become a focal point for infrastructure development and economic growth. If disaster mitigation measures do not accompany extensive infrastructure development, a future earthquake could replicate the disaster of 2006, potentially resulting in even more significant losses.

This research focuses on assessing the seismic vulnerability of soil in the YIA Underpass area as part of earthquake disaster mitigation efforts. Seismic vulnerability of soil refers to how soil can be affected or damaged by earthquakes. It can be influenced by various factors such as soil type, depth of the soil structure, the presence of groundwater, and the dynamic characteristics of the soil, such as shear wave velocity. Assessing the seismic vulnerability of soil is crucial in planning and evaluating existing building structures to minimize the risk and impact of destructive resonance caused by earthquakes. This assessment process is calculated based on natural frequency and amplification factors [4]. However, these data are unavailable in the research area, necessitating the use of microtremor observations to assess the seismic vulnerability of soil using the Horizontal-to-Vertical Spectral Ratio (HVSR) method.

The HVSR method is a technique for processing seismic wave data to determine the dynamic characteristics of the soil. Assuming that microtremors represent Rayleigh waves, the shear wave velocity of the soil can be calculated by inverting the HVSR curve. Shear wave velocity is critical for determining site classes and calculating seismic amplification of peak ground acceleration.

Several researchers have effectively used microtremor measurements to understand the dynamic characteristics of soil and assess its seismic vulnerability [5-11]. For instance, Noguchi et al. [5] clarified the damage caused by the 2018 East Hokkaido Iburi Earthquake through the HVSR method. Furthermore, microtremor surveys helped estimate landslide sediment layer thickness in three landslide areas of Tottori Prefecture, Japan [6]. Nishimura et al. [7] conducted microtremor investigations in the landslide area of Tandikat, West Sumatra, Indonesia, finding the predominant periods of the microtremor HVSR range between 0.1-0.4 s. Wijayanto et al. [8] also demonstrated how local conditions, particularly the landform effect, significantly influence V_{s30} in Gunungkidul, Yogyakarta, Indonesia. Asnawi et al. [9] successfully classified soil and developed a disaster mitigation plan utilizing the microtremor HVSR method in Lamteuba, Indonesia. Supriyadi et al. [10] studied the heritage area of Kota Lama Semarang, Indonesia, and enhanced their understanding of local seismic responses and resonance frequencies, which are crucial for spatial planning. In 2023, Wibowo et al. [11] utilized microtremor measurements and N-SPT data in the Opak River, Yogyakarta, Indonesia, area to determine seismic vulnerability characteristics.

This research aims to calculate the seismic vulnerability index (K_g) in the YIA Underpass area and its surroundings using the HVSR method. Other parameters such as natural frequency (f_0), shear wave velocity (V_s), soil classification, soil amplification, groundwater depth, and critical layer of soil susceptible to liquefaction are also discussed in this study.

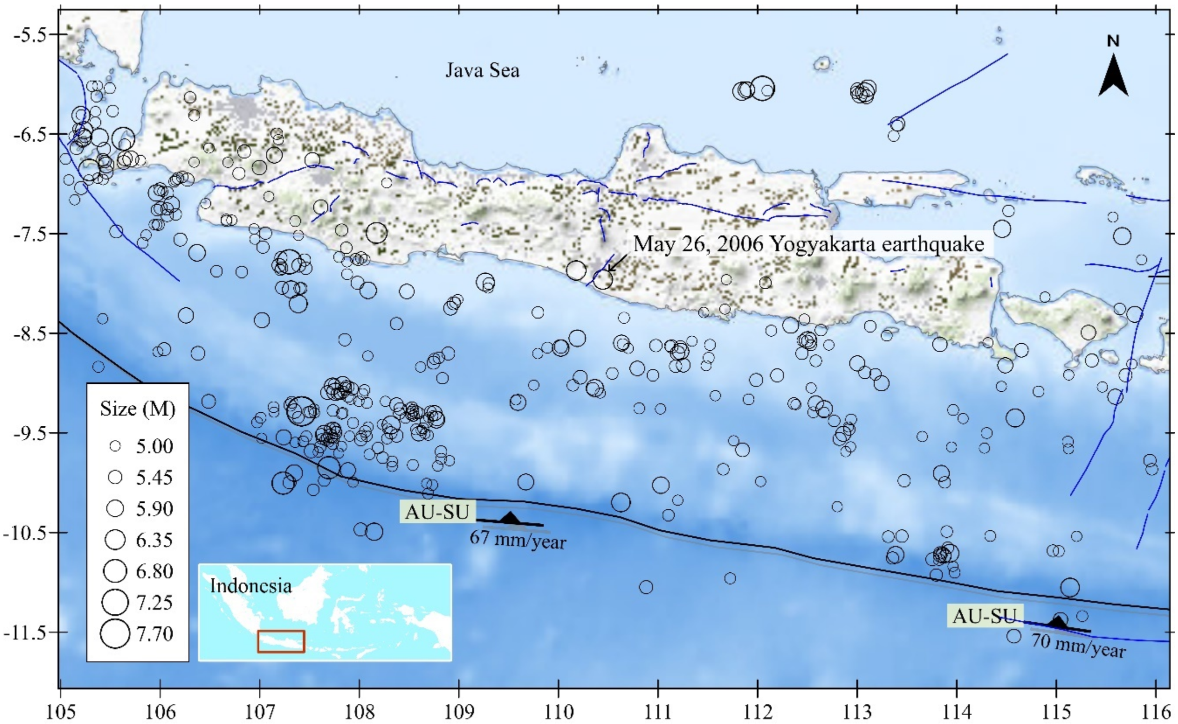

Fig.1 The seismicity map of earthquakes in Java Island and its surroundings for 2000-2023 (modified from [1]). The black line extending in the southern part of Java Island indicates a megathrust, and the blue line represents a fault line. The Australian-Sunda Plate (AU-SU) is subducting from the south to the north.

2. RESEARCH SIGNIFICANCE

The findings of this research make a valuable contribution to earthquake disaster mitigation efforts in the vicinity of the YIA Underpass. Understanding the seismic vulnerability index can minimize earthquake damage and loss risks. Structural damage due to resonance can also be prevented by knowing the dominant period of the soil. Soil classification and site amplification of peak ground acceleration values can be determined using the average shear wave velocity to a depth of 30 meters (V_{s30}). The results of this study are expected to serve as considerations and alternatives in assessing earthquake hazard potential and exploring dynamic soil characteristics.

3. GEOLOGICAL CONDITION

The research area is in the Temon District, Kulon Progo Regency, Yogyakarta Province, Indonesia. This region is characterized by low-lying terrain predominantly composed of Holocene alluvium deposits, as shown in Fig.2. Alluvium deposits are found along more significant streams and the coastal plain. The lithological conditions in the study area are characterized primarily by clean sands, with deposits downstream of the Bogowonto River containing barite minerals and iron sands [12].

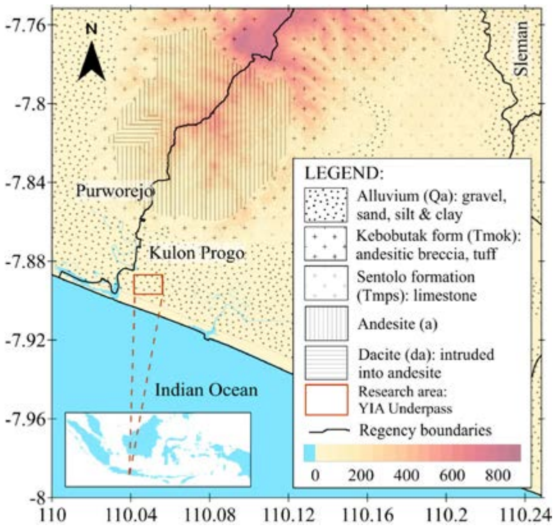

Fig.2 The geological conditions and elevation of the land in Kulon Progo and its vicinity (modified from [12-13])

4. METHOD

Microtremor refers to surface vibrations of the earth generated by various natural and anthropogenic vibration sources [14-15]. Microtremor is employed to discern the dynamic characteristics of subsurface soil layers, such as dominant frequencies and shear wave velocities. Groundwater depth measurements were used to identify critical layers with potential risk for liquefaction.

4.1 Measurement of Groundwater Depth

The measurement of groundwater depth was conducted using a simple method employing inextensible string, weights, and a measuring tape. Fig.3 provides a view of the observation well on the west side, which features a 5 cm diameter pipe. As illustrated in Fig.4, the observation wells were positioned outside the airport area on the west and east sides of the YIA Underpass.

Fig.3 Observation well on the western side

4.2 Microtremor Measurement

The acquisition, processing, and interpretation of microtremor data follow the guidelines of Site Effects Assessment Using Ambient Excitations (SESAME) [14]. These guidelines offer recommendations for conducting microzonation and site response studies.

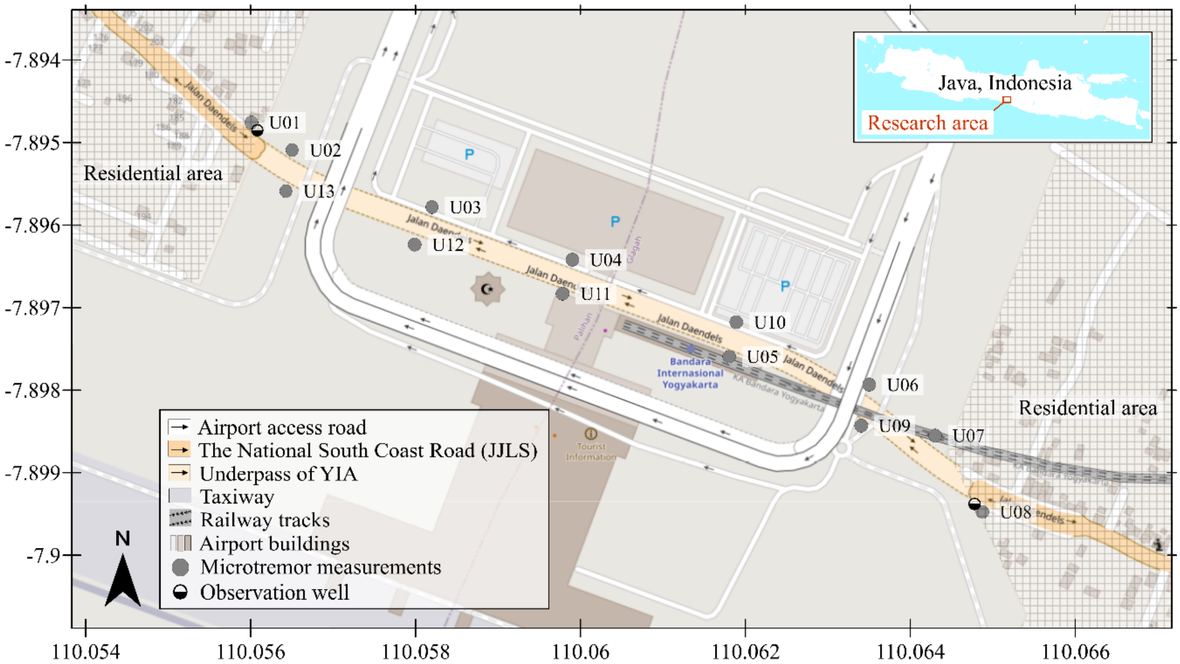

Fig.4 Map of microtremor measurement and observation site locations

Microtremor data acquisition was carried out at 13 points distributed along the YIA Underpass, as indicated in Fig.4. The YIA Underpass traverses the airport area. Points U01 and U08 are located outside the airport, while point U05 is between the underpass and the airport railway station. Microtremor measurements were performed using a single portable digital seismograph, with 30-45 minutes duration for each measurement point. The measurements took place on the night of March 16 and 17, 2023, to minimize excessive transient noise from sources such as airport train activity, flights, motor vehicles, and human activity. The measurement results are stored as mseed files.

The processing of mseed files utilized geopsy software [16]. Data processing involved the HVSR method, which calculates the amplitude ratio of horizontal and vertical Fourier spectra components. The output of the HVSR processing yields an HVSR curve.

Table 1 Reliability and clarity criteria for HVSR curve (modified from [14-15])

Criteria	SESAME
Reliability 1: f_0	$f_0 > 10 / l_w$
Reliability 2: $n_c = n_w. l_w. f_0$	$n_c > 200$
Reliability 3:	
if $f_0 > 0.5$ Hz, $f \in [0.5f_0, 2f_0]$, or	$\sigma_{A(f)} < 2$
if $f_0 < 0.5$ Hz, $f \in [0.5f_0, 2f_0]$	$\sigma_{A(f)} < 3$
Clarity 1: $f \in [0.25f_0, f_0]$	$A_{H/V(f)} < 0.5A_0$
Clarity 2: $f \in [f_0, 4f_0]$	$A_{H/V(f)} < 0.5A_0$
Clarity 3: A_0	$A_0 \geq 2$
Clarity 4: peak of SD curve f_0 $[A_{H/V(f)} + \sigma_{A(f)}]$; and peak SD curve f_0 $[A_{H/V(f)} - \sigma_{A(f)}]$	within $[0.95f_0, 1.05f_0]$
Clarity 5: if $f_0 < 0.2$ Hz	$\sigma f < 0.25f_0$
Clarity 5: if $f_0 \in [0.2, 0.5]$ Hz	$\sigma f < 0.20f_0$
Clarity 5: if $f_0 \in [0.5, 1.0]$ Hz	$\sigma f < 0.15f_0$
Clarity 5: if $f_0 \in [1.0, 2.0]$ Hz	$\sigma f < 0.10f_0$
Clarity 5: if $f_0 > 0.2$ Hz	$\sigma f < 0.05f_0$
Clarity 6: if $f_0 < 0.2$ Hz	$\sigma_{A(f0)} < 3.0$
Clarity 6: if $f_0 \in [0.2, 0.5]$ Hz	$\sigma_{A(f0)} < 2.5$
Clarity 6: if $f_0 \in [0.5, 1.0]$ Hz	$\sigma_{A(f0)} < 2.0$
Clarity 6: if $f_0 \in [1.0, 2.0]$ Hz	$\sigma_{A(f0)} < 1.78$
Clarity 6: if $f_0 > 0.2$ Hz	$\sigma_{A(f0)} < 1.58$

The HVSR curve must meet the criteria for reliability and have clear peaks to be interpretable. Table 1 outlines the criteria for assessing the reliability and clarity of the HVSR curve. The HVSR curve must satisfy all three reliability criteria and at least five clarity criteria to be interpretable.

In Table 1, f_0 represents peak frequency (Hz), A_0 denotes HVSR peak amplitude at f_0, l_w signifies window length (in seconds), n_w indicates the number of windows selected for the average HVSR curve, n_c represents the number of significant cycles, f stands for the current frequency, $\sigma_A(f)$ is the standard deviation of $A_{H/V}(f)$ at f, $A_{H/V}(f)$ is HVSR curve amplitude at frequency f, σ_f is standard deviation of H/V peak frequency ($f_0 \pm \sigma_f$), $\sigma_A(f_0)$ is the standard deviation of $A_{H/V}(f)$ at f_0, and SD refers to standard deviation.

4.3 HVSR Curve Analysis

4.3.1 Seismic vulnerability index (K_g)

The seismic vulnerability index (K_g) is a parameter used to quantify the potential damage caused by earthquakes. Soil has a high potential for substantial damage when the seismic vulnerability index value exceeds 20. The risk of damage decreases when the seismic vulnerability index value is less than 20 [4]. The seismic vulnerability index can be calculated using Eq. (1).

$$K_g = \frac{{A_0}^2}{f_0} \tag{1}$$

Where K_g is the seismic vulnerability index of soil, f_0 is the dominant frequency of soil, and A_0 is the peak amplitude value of the HVSR curve at f_0.

4.3.2 Shear wave velocity (V_s)

The average shear wave velocity to a depth of 30 meters is a crucial parameter for calculating the amplification factor of peak ground acceleration at the ground surface based on site class. It can be calculated using Eq. (2).

$$V_{s30} = \frac{30}{\sum_{i=1}^{N}\left(\frac{h_i}{V_{si}}\right)} \tag{2}$$

Where V_{s30} is the average shear wave velocity of soil to a depth of 30 meters (m/s), N is the number of soil layer thicknesses, h_i is the thickness of soil layers (m), and V_{si} is the shear wave propagation velocity at the depth of the reviewed soil (m/s).

The shear wave velocity value (V_s) is obtained through the inversion of the HVSR curve using the ellipticity curve method in the dinver program, an additional plugin in geopsy. The dinver program employs a neighborhood algorithm and Monte Carlo calculation techniques [17].

4.3.3 Site class

The site classification is determined based on soil conditions down to 30 meters in the field. Table 2 shows the soil classifications by V_{s30}.

Table 2 Site soil classes (modified from [18])

Class	Profile	V_{s30} (m/s)
SA	Hardrock	> 1500
SB	Bedrock	750 - 1500
SC	Stiff soil	350 - 750
SD	Medium soil	175 - 350
SE	Soft soil	< 175

4.3.4 Stress-corrected shear wave velocity (V_{s1})

The stress-corrected shear wave velocity is the shear wave velocity of soil corrected for overburden pressure. Overburden pressure calculation assumes soil density above the groundwater level at 1.76 Mg/m^3 and 1.92 Mg/m^3 below the groundwater level [19]. The stress-corrected shear wave velocity value can be calculated using Eq. (3).

$$V_{s1} = V_s \left(\frac{P_a}{\sigma'_v}\right)^{0.25} \quad (3)$$

Where V_{s1} is the stress-corrected shear wave velocity (m/s), V_s is the shear wave velocity of soil (m/s), P_a represents atmospheric pressure or reference pressure (100 kPa), and σ'_v is the effective stress of soil at the reviewed depth (kPa).

5. RESULT AND DISCUSSION

5.1 Groundwater Table (GWT)

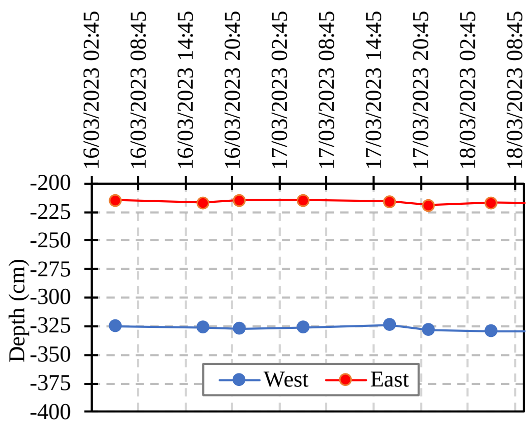

Fig.5 Groundwater depth (clear weather, no rain)

The groundwater depth on the eastern side is shallower compared to the western side, as shown in Fig.5. The highest groundwater level in the observation well on the western side is 324 cm, while on the eastern side, it is 215 cm. This difference may be attributed to variations in ground elevation. The elevation of the observation well on the western side is ± 605 mm higher than that on the eastern side from the ground surface.

The research area is situated within the discharge area of the Wates groundwater basin, where water flows from the north to the south and east. The study area is assessed to have a high potential for liquefaction due to its shallow groundwater, thick sandy sediments, and high seismic activity [20].

5.2 Seismic Vulnerability Analysis

Geopsy automatically generates the HVSR curve (Fig.6). Table 3 presents the assessment results of the HVSR curves based on the criteria outlined in Table 1. The assessment results indicate that five HVSR curves do not meet the requirements, while eight HVSR curves meet the criteria. Based on the HVSR curves that meet the requirements, the dominant frequencies (f_0) range from 0.21 to 0.29 Hz, and the amplification factors (A_0) vary from 2.64 to 5.58.

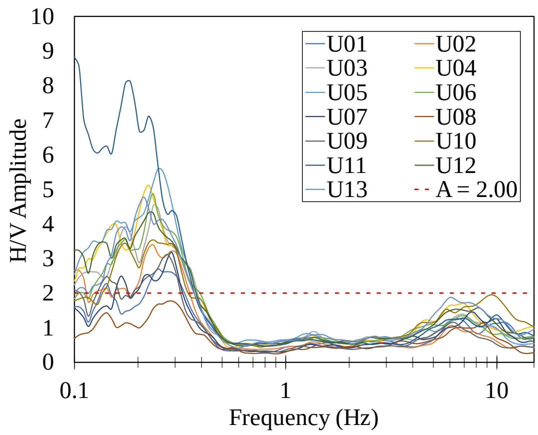

Fig.6 HVSR curves

Values for the seismic vulnerability index and shear wave velocity of the soil to a depth of 30 meters were determined using Eq. (1) and Eq. (2), as shown in Table 4. The dominant frequency of soil (f_0), which correlates with the depth of soil layers, is larger in hard soil and smaller in softer soil. The research area exhibits low-frequency values, confirming thick alluvial sediment deposits at the YIA Underpass and its vicinity. These sediment deposits have the potential to amplify seismic vibrations and associated damage. Tall building structures and long single-span bridge structures are more susceptible to low dominant frequencies due to resonance unless they are designed to be stiffer.

All measured points have seismic vulnerability indices exceeding 20 (Table 4), with the peak values observed at sites U04 and U05. The high values of the seismic vulnerability index further demonstrate the vulnerability of the soil to seismic activity. Point U05 is between the underpass and the airport railway station, while point U04 is south of the airport parking area. Gridding was performed using Kriging interpolation techniques to estimate the spatial distribution of the seismic vulnerability index around the microtremor measurement points, as shown in Fig.7.

Table 3 Assessment of HVSR curves

Site	Reliability 1	Reliability 2	Reliability 3	Clarity 1	Clarity 2	Clarity 3	Clarity 4	Clarity 5	Clarity 6	Result
U01	0.249 > 0.167	239 > 200	0.629 < 3	1.296 < 1.322	0.278 < 1.322	2.645 > 2.00	0.219 & 0.296 $\notin[f_0\pm5\%]$	0.031 < 0.050	0.975 < 2.5	Passed
U02	0.236 > 0.167	227 > 200	0.748 < 3	1.739 ≮ 1.531	0.369 < 1.531	3.061 > 2.00	0.211 & 0.300 $\notin[f_0\pm5\%]$	0.036 < 0.047	1.219 < 2.5	Failed
U03	0.227 > 0.200	159 ≯ 200	0.836 < 3	2.240 ≮ 1.996	0.483 < 1.996	3.992 > 2.00	0.114 & 0.176 $\notin[f_0\pm5\%]$	0.036 < 0.045	1.258 < 2.5	Failed
U04	0.225 > 0.111	202 > 200	0.962 < 3	2.347 < 2.533	0.415 < 2.533	5.066 > 2.00	0.189 & 0.263 $\notin[f_0\pm5\%]$	0.032 < 0.045	1.036 < 2.5	Passed
U05	0.249 > 0.167	224 > 200	1.352 < 3	2.531 < 2.788	0.547 < 2.788	5.575 > 2.00	0.218 & 0.282 $\notin[f_0\pm5\%]$	0.026 < 0.050	1.500 < 2.5	Passed
U06	0.236 > 0.167	369 > 200	0.918 < 3	1.836 < 2.150	0.463 < 2.150	4.299 > 2.00	0.208 & 0.288 $\notin[f_0\pm5\%]$	0.033 < 0.047	2.314 < 2.5	Passed
U07	0.289 > 0.167	226 > 200	0.845 < 3	1.030 < 1.321	0.288 < 1.321	2.642 > 2.00	0.231 $\notin[f_0-5\%]$; 0.296 $\in[f_0+5\%]$	0.027 < 0.058	1.371 < 2.5	Passed
U08	0.289 > 0.200	145 ≯ 200	0.440 < 3	0.697 < 0.880	0.248 < 0.880	1.761 ≯ 2.00	0.239 & 0.317 $\notin[f_0\pm5\%]$	0.032 < 0.058	0.486 < 2.5	Failed
U09	0.275 > 0.167	215 > 200	0.830 < 3	1.329 < 1.514	0.297 < 1.514	3.029 > 2.00	0.219 & 0.311 $\notin[f_0\pm5\%]$	0.038 < 0.055	1.156 < 2.5	Passed
U10	0.236 > 0.182	208 > 200	0.766 < 3	1.674 < 1.747	0.439 < 1.747	3.494 > 2.00	0.200 & 0.285 $\notin[f_0\pm5\%]$	0.035 < 0.047	1.440 < 2.5	Passed
U11	0.184 > 0.125	235 > 200	1.641 < 3	6.037 ≮ 3.637	0.519 < 3.637	7.274 > 2.00	0.158 & 0.234 $\notin[f_0\pm5\%]$	0.031 < 0.046	3.157 ≮ 3.0	Failed
U12	0.225 > 0.167	310 > 200	0.772 < 3	2.572 ≮ 2.127	0.465 < 2.127	4.254 > 2.00	0.185 & 0.258 $\notin[f_0\pm5\%]$	0.030 < 0.045	1.537 < 2.5	Failed
U13	0.214 > 0.167	205 > 200	0.970 < 3	1.985 < 2.163	0.414 < 2.163	4.326 > 2.00	0.185 & 0.271 $\notin[f_0\pm5\%]$	0.035 < 0.043	1.367 < 2.5	Passed

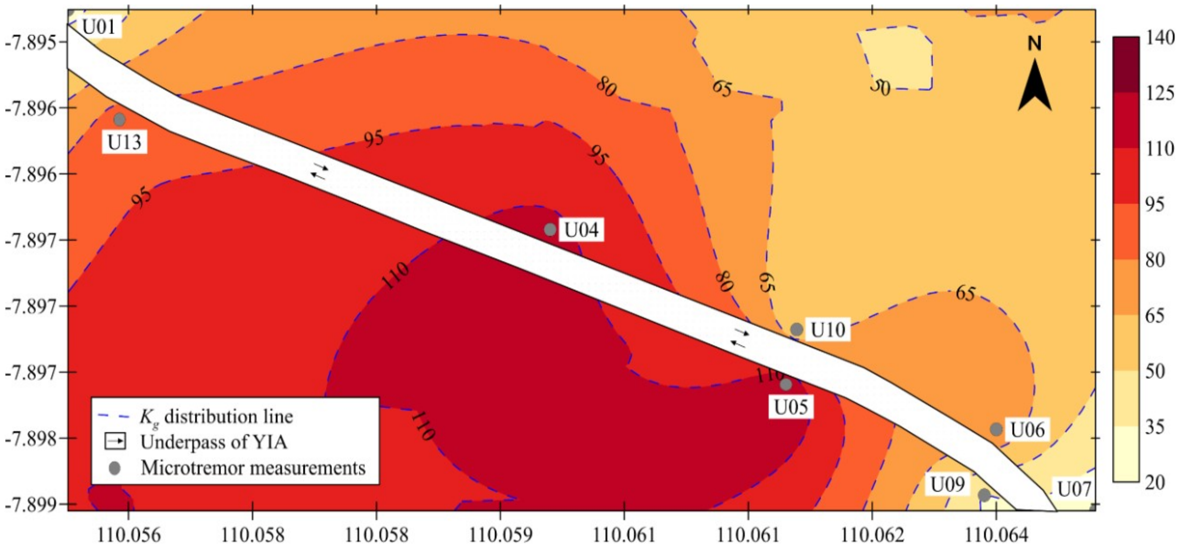

Fig.7 Seismic vulnerability index (K_g) distribution

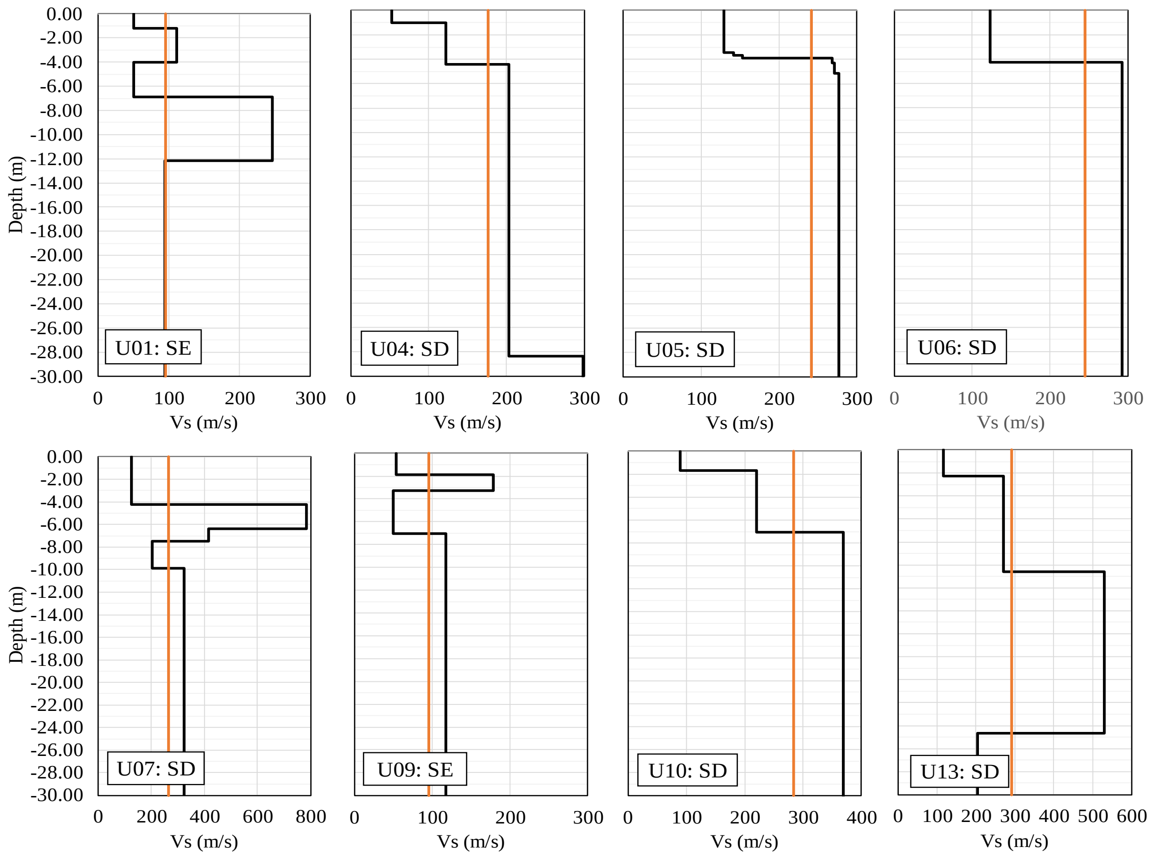

Fig.8 The shear wave propagation velocity (black line), the average shear wave velocity to a depth of 30 meters (red line), and the soil site class

Table 4 Results of HVSR curve analysis

Site	f_0 (Hz)	A_0	T_0 (s)	Eq. (1)	Eq. (2)	Class
U01	0.25	2.65	4.02	28.10	95.12	SE
U04	0.23	5.07	4.44	114.06	176.08	SD
U05	0.25	5.58	4.02	124.82	241.96	SD
U06	0.24	4.30	4.24	78.31	244.88	SD
U07	0.29	2.64	3.46	24.15	265.63	SD
U09	0.28	3.03	3.64	33.36	95.90	SE
U10	0.24	3.49	4.24	51.73	284.42	SD
U13	0.21	4.33	4.67	87.45	291.49	SD

Fig.8 shows the shear wave velocity profile of the soil and site class. While points U04 and U05 exhibit higher seismic vulnerability indices than the others, the average shear wave velocity to a depth of 30 meters (V_{s30}) for points U01 and U09 is lower, which places them in the SE site class. The soil site class is essential for determining the magnitude of peak ground acceleration amplification.

Fig.9 shows the seismic amplification of peak ground acceleration values for SD and SE soil site classes. The amplification factors can be calculated based on the soil site class and the peak ground acceleration (PGA) or spectral acceleration at the bedrock (SA). Based on the USGS shakemap for the Yogyakarta earthquake on May 26, 2006, the research area has a potential for light to moderate seismic hazard [1]. The estimated horizontal peak ground acceleration is 0.20 g. If the PGA value is 0.20 g, the amplified peak ground acceleration at the surface (PGA_M) is 1.4 times for the SD site class and 1.7 times for the SE site class. The soil site class also provides different amplification values for horizontal spectral response at 1.0 second (F-SA), with the SE site class having higher amplification than the SD class.

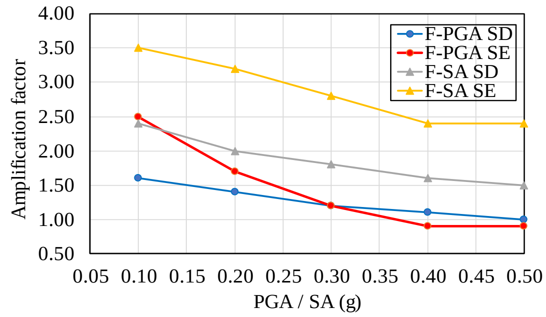

Fig.9 Amplification factors of peak ground acceleration (modified from [18])

5.3 Liquefaction Hazard Potential

Liquefaction occurs in water-saturated, loose, sandy soils when they lose their stiffness and strength due to seismic activity. Liquefaction is not likely to occur in clean sands with a stress-corrected shear wave velocity (V_{s1}) exceeding 215 m/s [19]. Based on Eq. (3), the soil capacity was analyzed at points U01, U05, and U07, as shown in Fig.10, with their locations depicted in Fig.4. Point U01 was selected due to its SE site class and groundwater depth of 215 cm from the ground surface. Point U05 was chosen for its highest seismic vulnerability index value. Point U07 was selected to examine the resistance to liquefaction on the eastern side.

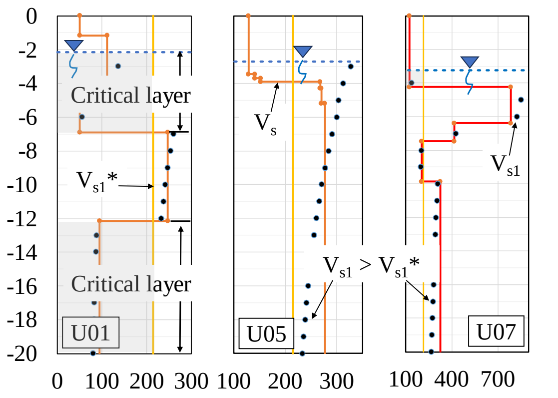

Fig.10 Critical layers with liquefaction potential

Fig.10 reveals that point U05 is the most resistant to liquefaction hazard because it has a V_{s1} value exceeding 215 m/s. Point U01 is the most vulnerable to liquefaction hazard as V_{s1} in some soil layers is less than 215 m/s. These critical layers are determined based on soil layers with V_{s1} less than 215 m/s and are saturated with water [19]. All measurement points exhibit a high seismic vulnerability index, but not all have the liquefaction potential.

6. CONCLUSION

This research underscores the importance of understanding soil dynamic characteristics to assess the seismic vulnerability of soil. The seismic vulnerability index (K_g) values in the YIA Underpass and its surrounding areas exceed 20, indicating a high potential for seismic hazards.

Based on the interpretation of geological conditions and the HVSR curve, the research area is characterized by low dominant frequencies (f_0) ranging from 0.214 to 0.289 Hz. This analysis suggests that the research area comprises thick soil sediment deposits. These sediment deposits can amplify peak ground acceleration, increasing the risk of damage during seismic events. To avoid structural resonance damage, ensure that building frequencies do not coincide with the dominant frequencies of soil.

The inversion of the HVSR curve reveals variable shear wave velocities. The V_{s30} calculations classify six points into the SD class (medium soil), whereas points U01 and U09 are categorized as SE class (soft soil) due to V_{s30} values under 175 m/s.

Furthermore, considering that all points have shallow groundwater levels, and based on the stress-corrected shear wave velocity (V_{s1}), point U01 is identified as more susceptible to liquefaction than U05 and U07, as V_{s1} in some soil layers is less than 215 m/s. Further research on seismic hazards and their implications is recommended for soil layers with V_{s1} less than 215 m/s.

7. ACKNOWLEDGMENTS

The authors thank the Ministry of Public Works and People's Housing as the project owner, PT. Angkasa Pura I for granting permission to conduct microtremor measurements, and the Meteorology, Climatology, and Geophysics Agency for their support in providing personnel and equipment.

8. REFERENCES

[1] United States Geological Survey (USGS), Earthquake Maps, A web page accessed from: https://earthquake.usgs.gov/earthquakes/map.

[2] The Ministry of National Development Planning of Indonesia (BAPPENAS), Preliminary Damage and Loss Assessment Yogyakarta and Central Java Natural Disaster, A Joint Report of BAPPENAS, the Provincial and Local Governments of D. I. Yogyakarta, the Provincial and Local Governments of Central Java, and International Partners, 2006, pp.1-141.

[3] The Government of Kulon Progo Regency, Regulation of the Regent of Kulon Progo No. 47 of 2023 on the Detailed Spatial Plan of the Area Surrounding Yogyakarta International Airport for the Years 2023-2043, Legal and Documentation Information Network of Kulon Progo Regency, 2023, pp.1-71.

[4] Nakamura Y., On The H/V Spectrum, In Proceedings of the 14th World Conference on Earthquake Engineering in Beijing, China, 2008, pp.1-10.

[5] Noguchi T., Nishimura I., Ono Y., and Kohno M., Estimation of Subsurface Structure Based on Microtremor and Seismic Observations in Area Damaged by 2018 Hokkaido Eastern Iburi Earthquake, Hokkaido, Japan, International Journal of GEOMATE, Vol. 20, Issue 81, 2021, pp.8-15.

[6] Noguchi T., Nishimura I., and Kagawa T., Estimation of Subsurface Structure of Landslide Area Based on Microtremor Observation in The Hojoshima, Nawashiro and Amedaki Area, Tottori, Japan, International Journal of GEOMATE, Vol. 21, Issue 88, 2021, pp.48-53.

[7] Nishimura I., Noguchi T., Ono Y., and Kohno M., Subsurface Structures Based on Microtremor Observations in Landslide Area of Tandikat, West Sumatra, Indonesia, International Journal of GEOMATE, Vol 22, Issue 90, 2022, pp.57-62.

[8] Wijayanto, Mardiatno D., Nehren U., Marfai M. A., and Pramono S., Spatial Distribution of Vs30 Based on MASW and HVSR Inversion in Gunungkidul, Yogyakarta, International Journal of GEOMATE, Vol. 22, Issue 94, 2022, pp.29-38.

[9] Asnawi Y., Simanjuntak A., Muksin U., Rizal S., Syukri M., Maisura M., and Rahmati R., Analysis of Microtremor H/V Spectral Ratio and Public Perception for Disaster Mitigation, International Journal of GEOMATE, Vol. 23, Issue 97, 2022, pp.123-130.

[10] Supriyadi, Khumaedi, Sugiyanto, Fadilah A. R., and Muttaqin W. H., Study of The Subsurface Structure Based on Microseismic Data in The Heritage Area of Kota Lama Semarang, Indonesia, International Journal of GEOMATE, Vol. 23, Isuue 97, 2022, pp.211-219.

[11] Wibowo N. B., Fathani T. F., Pramumijoyo S., and Marliyani G. I., Microzonation of Seismic Parameters in Geological Formation Units Along the Opak River Using Microtremor Measurements, International Journal of GEOMATE, Vol. 25, Issue 110, 2023, pp.208-219.

[12] Rahardjo W., Sukandarrumidi, and Rosidi H.M.D., Geological Map of The Yogyakarta Sheet, Jawa, Center for Geological Survey Geological Agency Ministry of Energy and Mineral Resources, 2012, pp.1-1.

[13] Geospatial Information Agency of Indonesia, Digital Land Map of Indonesia, A web page accessed from: https://tanahair.indonesia.go.id/.

[14] Site Effects Assessment Using Ambient Excitations (SESAME), Guidelines for The Implementation of The H/V Spectral Ratio Technique on Ambient Vibrations Measurements Processing and Interpretation, SESAME European Research Project, WP12 – Deliverable D23.12 European Commission Research General Directorate, Project No. EVG1-CT-200-00026, 2004, pp.1-62.

[15] Molnar S., Sirohey A., Assaf J., Bard P. Y., Castellaro S., Cornou C., Cox B., Guillier B., Hassani B., Kawase H., Matsushima S., Sánchez-Sesma F. J., and Yong A., A Review of The Microtremor Horizontal-to-Vertical Spectral Ratio (MHVSR) Method, Journal of Seismology, Vol. 26, No. 4, 2022, pp.653-685.

[16] Wathelet M., Chatelain J. L., Cornou C., Di Giulio G., Guillier B., Ohrnberger M., and Savvaidis A., Geopsy: A User-Friendly Open-Source Tool Set for Ambient Vibration Processing, Seismological Research Letters, Vol. 91, No. 3, 2020, pp.1878-1889.

[17] Wathelet M., An Improved Neighborhood Algorithm: Parameter Conditions and Dynamic Scaling, Geophysical Research Letters, Vol. 35, Issue 9, 2008, pp.1-5.

[18] National Standardization Agency of Indonesia, SNI 8460:2017 Geotechnical Design Requirements, BSN, 2017, pp.1-323.

[19] Andrus R. D. and Stokoe II K. H., Liquefaction Resistance of Soils from Shear-Wave Velocity, Journal of Geotechnical and Geoenvironmental Engineering, Vol. 126, No. 11, 2000, pp.1015-1025.

[20] Ilham M. and Putra D. P. E., Integrated Mapping of the Earthquake-Induced Liquefaction in Wates Groundwater Basin, Kulon Progo for Land Use Planning Consideration: A Preliminary Study, In IOP Conference Series: Earth and Environmental Science, Vol. 1071, No. 1, 2021, pp.1-12.